

CART: Compositional Auto-Regressive Transformer for Image Generation

Siddharth Roheda
 Samsung Research Institute
 Bangalore, India
 sid.roheda@samsung.com



Figure 1. Top: Generation process of the CART model. Bottom: Generated image samples using CART

Abstract

In recent years, image synthesis has achieved remarkable advancements, enabling diverse applications in content creation, virtual reality, and beyond. We introduce a novel approach to image generation using Auto-Regressive (AR) modeling, which leverages a “next-detail” prediction strategy for enhanced fidelity and scalability. While AR models have achieved transformative success in language modeling, replicating this success in vision tasks has presented unique challenges due to the inherent spatial dependencies in images. Our proposed method addresses these challenges by iteratively adding finer details to an image compositionally, constructing it as a hierarchical combination of base and detail image factors. This strategy is shown to be more effective than the conventional “next-token” prediction and even surpasses the state-of-the-art “next-scale” prediction approaches. A key advantage of this method is its scalability to higher resolutions without requiring full model retraining, making it a versatile solution for high-resolution image generation.

1. Introduction

Recent advancements in Generative AI for image synthesis and editing have garnered significant interest within both research and industry sectors. Conventional approaches in Generative AI, including Generative Adversarial Networks (GANs) [13, 27] and Variational Autoencoders (VAEs) [20, 37], typically aim to produce entire scenes in a single pass. However, human perception and understanding of visual scenes are inherently compositional. For example, when creating a scene, an artist typically follows an iterative process, beginning with rough outlines, refining shapes, and gradually adding details and shading. Generating entire scenes in one attempt can preclude this iterative addition of detail, posing challenges in scaling to high-resolution images.

Recent research has introduced step-wise approaches to the image generation problem, where each step incorporates a subset of details. For instance, diffusion-based methods [15, 38] initiate with a noisy vector and employ a denoising model to incrementally remove noise, progressively revealing a coherent image. Similarly, auto-regressive (AR) mod-

els [14, 29, 35, 40] tackle image generation in a patch-wise manner, further supporting an iterative image generation approach. Specifically, AR models in image generation, such as VQGAN [12] and DALLE [32], aim to parallel the success of AR-based models in large language models (LLMs). These models use visual tokenizers that convert continuous images into grids of 2D tokens, enabling AR models to learn next-token prediction.

Despite the success of AR methods in natural language processing, replicating similar advancements in computer vision has proven challenging. Recent studies in AR modeling [39] indicate that the sequence in which image tokens are processed during AR learning can substantially affect model performance.

In this paper, we introduce a novel Auto-Regressive Image Generation approach that constructs high-quality images by progressively assembling a scene in a hierarchical manner. The process begins with the creation of a smooth base image, which is then enhanced through iterative addition of finer details, resulting in a coherent final image (see Figure 1). This method closely emulates a human approach to image creation—starting with a foundational sketch and refining it with increasing levels of detail. Our approach first decomposes a training image into “base” and “detail” components using an edge-aware smoothing technique. These components are then encoded into multi-scale detail token maps. The Auto-Regressive process initiates with a 1×1 token, predicting successive token-maps to construct the base component of the image. Once the base is established, the model transitions to predicting the detail components, incrementally layering them to enhance the base image. This structured, iterative process aligns with a natural order of image formation, enhancing both quality and interpretability in the generation process.

The **Contributions** of this paper include:

- A novel approach enabling iterative image composition which aligns well with the natural order of image formation.
- A tokenization approach that performs quantization of the image decomposition into a base layer and multiple detail layers
- High-resolution image generation without the need for model retraining, demonstrating scalability and adaptability to higher resolutions.

2. Related Work

2.1. Generative Models

Generative models for image synthesis have evolved at a rapid pace over the last decade. Image generation can be performed either unconditionally or by conditioning the model on some prior information such as text, class label, etc. Variational Auto Encoders (VAEs) [20, 37], and Gen-

erative Adversarial Networks (GANs) [13, 27] have revolutionized the space of Image Generation. GANs train a generator and discriminator network in an adversarial fashion. These models are capable of generating realistic, high quality images in a single step.

The more recent Diffusion models [15, 16, 38] are based on a sequential denoising process that gradually transforms a noise-perturbed image into a realistic sample, effectively learning the data distribution by reversing a predefined noising process. This approach allows diffusion models to produce high-quality images and fine-grained textures, which has established them as a strong alternative to Generative Adversarial Networks (GANs) and other generative methods. Diffusion models are highly flexible and have been applied to a variety of generative tasks beyond image synthesis, including text-to-image generation [46, 49], inpainting [9, 25, 43], super-resolution [23, 45], 3D reconstruction [3, 48], and generalized image editing [5, 19]. However, despite their strengths, diffusion models typically require a substantial number of iterative steps to generate high-quality images, which can lead to long generation times, especially for high-resolution images. This computational overhead has limited their scalability for applications that demand efficient, real-time synthesis.

2.2. Auto-Regressive Generative Models

Auto-Regressive (AR) models attempt to predict the next token in a sequence while conditioning on the previous tokens of the sequence. Recent years have seen the rise of AR models. Specifically the Generative Predictive Text (GPT) [6, 31] used transformers [42] to learn Large Language Models (LLMs) which led to a significant performance improvement in tasks like language generation, prediction and understanding. Many works have attempted to replicate this success of AR models in CV applications including image generation. One of the first works to do this was DRAW [14], where a sequential variational auto-encoding framework was used with Recurrent Neural Networks (RNN) [26] as the building blocks. Another approach in AR generative modelling was to predict the pixels of the image in a raster-scan fashion (Pixel CNN [35], Pixel RNN [40] and Image Transformer [29]). Limitation of such models lies in the computational complexity required to predict a real image with billions of pixels. A large Image-GPT [8] model with 6.8B parameters was only capable of predicting a 96×96 image. To alleviate this problem, Vector Quantized Variational Auto Encoder (VQ-VAE) [41] was introduced, where an encoder was used to compress the image into a low-dimensional latent space, followed by quantization to discretize the latent space into tokens which are predicted by an AR model. Recent work [29] has trained transformer based decoder to auto-regressively generate a realistic image using quantized tokens from the VQ-VAE. In [39], the

authors note that the ordering of tokens is critical when it comes to AR modelling for image generation, and propose a multi-scale approach to tokenization. Instead of using the standard next-token prediction scheme, the authors adopt a next-scale prediction scheme, where the image at higher resolution is predicted at each time-step.

2.3. Vector Quantized VAE

In order to perform Auto-Regressive modeling to images via next-token prediction, the image must be tokenized into discrete tokens. This is achieved by using a quantized auto-encoder such as [41]. The image is first converted to a feature map $f \in \mathbb{R}^{h \times w \times C}$,

$$f = \mathcal{E}(I), \quad (1)$$

where, $\mathcal{E}(\cdot)$ is the encoder. Following this, the feature map is converted to discrete tokens, $q \in [V]^{h \times w}$,

$$q = \mathcal{Q}(f), \quad (2)$$

where \mathcal{Q} is the quantizer. The quantizer typically consists of a learnable codebook $\mathcal{Z} \in \mathbb{R}^{V \times C}$ with V vectors. Each code index $q^{(i,j)}$ is mapped from each feature vector $f^{(i,j)}$ as,

$$q^{(i,j)} = (\arg \min_{v \in [V]} \|\text{look-up}(\mathcal{Z}, v) - f^{(i,j)}\|_2) \in [V], \quad (3)$$

where $\text{look-up}(\mathcal{Z}, v)$ refers to taking the v^{th} vector in codebook \mathcal{Z} . To train the quantized autoencoder, \mathcal{Z} is looked up by every $q^{(i,j)}$ to get \hat{f} , which is the approximation of f . Then, a new image, \hat{I} is reconstructed by the decoder $\mathcal{D}(\cdot)$ given \hat{f} ,

$$\hat{f} = \text{look up}(\mathcal{Z}, q) \quad (4)$$

$$\hat{I} = \mathcal{D}(\hat{f}). \quad (5)$$

A compound loss, \mathcal{L} is minimized,

$$\|I - \hat{I}\|_2 + \|f - \hat{f}\|_2 + \lambda_p \mathcal{L}_p(\hat{I}) + \lambda_G \mathcal{L}_G(\hat{I}), \quad (6)$$

where \mathcal{L}_p is a perceptual loss like LPIPS [47], \mathcal{L}_G is a discriminative loss such as the StyleGAN discriminator loss [18], and λ_p and λ_G are the corresponding loss weights.

2.4. Mumford-Shah Functional

The Mumford-Shah functional [28] provides a form of all regularizers which aim at combining smoothing of edges with enhancement of edges. Given a bounded open set $\Omega \in \mathbb{R}$, $d \geq 1$, the vectorial Mumford-Shah problem is given by,

$$\min_{u,K} \int_{\Omega} |u - f|^2 dx + \alpha \int_{\Omega} |\nabla u|^2 dx + \lambda |K|, \quad (7)$$

where $f : \Omega \rightarrow \mathbb{R}^k$ is a vector-valued input image with $k \geq 1$ channels. This model approximates f by a function $u : \Omega \rightarrow \mathbb{R}^k$ which is smooth everywhere except for a possible $(d - 1)$ dimensional jump set K , at which u is discontinuous. The weight $\lambda > 0$ controls the length of K . The limiting case $\alpha \rightarrow \infty$ imposes zero gradient outside K and is known as the piecewise constant Mumford-Shah model.

One of the most common approaches for solving the Mumford-Shah functional for images is the Ambrosio-Tortorelli Approach [2] which is given by,

$$\min_{u,s} \int_{\Omega} |u - f|^2 dx + \alpha \int_{\Omega} (1 - s)^2 |\nabla u|^2 dx + \lambda \int_{\Omega} (\epsilon |\nabla s|^2 + \frac{1}{4\epsilon} s^2) dx, \quad (8)$$

with a small parameter $\epsilon > 0$ and an additional variable $s : \Omega \rightarrow \mathbb{R}$. The key idea is to introduce s as an edge set indicator, in the sense that points $x \in \Omega$ are part of the edge set K if $s(x) \approx 1$ and part of smooth region if $s(x) \approx 0$. The variables u and s are found by alternating minimization.

3. Proposed Approach

We propose a novel approach in which the model initially predicts a smooth, piecewise-constant base image, subsequently refining it through iterative addition of details. Our training methodology comprises three key steps:

- **Decomposition:** Each training image is decomposed into n hierarchical base-detail factors, representing progressive layers of detail.
- **Encoding and Tokenization:** The factors are encoded into a latent space using a Vector Quantized Variational Auto-Encoder (VQ-VAE), preserving essential features while reducing dimensionality.
- **Iterative Prediction:** A Transformer decoder architecture is trained to predict the successive detail factor (token-map) of the image, enabling controlled and incremental addition of details.

3.1. Hierarchical Base-Detail Decomposition

An image can be represented as a linear combination of factor images, where each factor captures distinct properties of the image. In our framework, we decompose an image into a base and a detail factor, represented as

$$I = B + D, \quad (9)$$

where, $I \in \mathbb{R}^{H \times W \times 3}$ denotes an image from the training set and $B \in \mathbb{R}^{H \times W \times 3}$ and $D \in \mathbb{R}^{H \times W \times 3}$ denote the base and detail factors, respectively. The base factor B is obtained by minimizing the Mumford-Shah functional

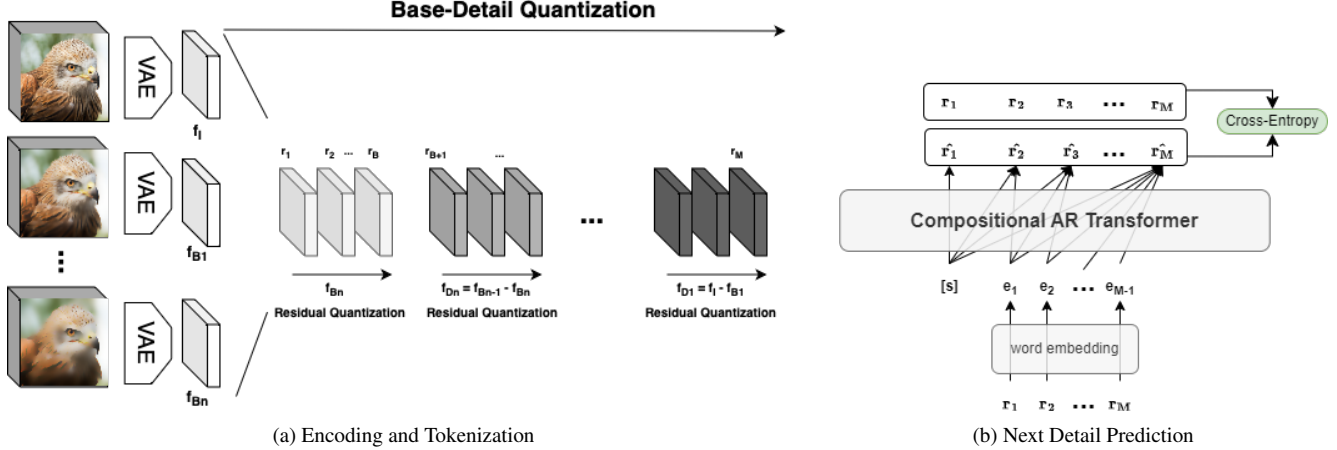


Figure 2. Overview of the CART Approach.

through the Ambrosio-Tortorelli approach, as detailed in Equation 8. This base factor can be recursively decomposed to yield multiple detail factors, leading to an expression of the form

$$I = B_n + D_n + D_{n-1} + \dots + D_1, \quad (10)$$

where, $B_{k-1} = B_k + D_k, \forall k \in \{1, \dots, n\}$. Equation 10 defines the n^{th} order decomposition of I . In this decomposition, the base factor B_n captures the image’s overall structure, composition, and global features, while the detail factors $\{D_k\}_{k=1}^n$ represent local features that contribute to the finer details of the image. Figure 3 (a) shows the hierarchical base-detail decomposition process. Figure 3 (b) depicts how the Image I is represented by the base and detail factors in a vector form.

3.2. Encoding and Tokenization

In our approach, each image is represented by token maps $\{r_1, r_2, \dots, r_{\mathcal{M}}\}$ within the latent space of a Vector Quantized Variational Autoencoder (VQ-VAE), rather than single tokens. This token-map representation preserves the spatial coherence of the feature map and reinforces the spatial structure inherent in the image. We propose a tokenization scheme such that these token maps represent the base and detail factors. Specifically, the image representation is comprised of \mathcal{B} base token maps, $(r_1, \dots, r_{\mathcal{B}})$, where $\mathcal{B} < \mathcal{M}$ and $(\mathcal{M} - \mathcal{B})$ detail token maps, $(r_{\mathcal{B}+1}, \dots, r_{\mathcal{M}})$.

Following the Base-Detail Decomposition, we encode the original image I along with the Base Factors $\{B_k\}_{k=1}^n$ using a VAE,

$$f_{B_k} = \mathcal{E}(B_k), \quad (11)$$

where $f_{B_k} \in \mathbb{R}^{h \times w \times c} \forall k \in \{1, \dots, n\}$. As in previous work [39], token maps, rather than individual tokens, are

utilized, achieved by performing residual quantization [22] on the encoded feature map f_{B_n} with a quantization depth of \mathcal{B} to get the base factor token maps $\{r_1, \dots, r_{\mathcal{B}}\}$. The encoded representation of k^{th} detail factor is then determined as follows,

$$f_{D_k} = f_{B_{k-1}} - f_{B_k}, \quad (12)$$

where, f_{B_k} is the encoded representation of the k^{th} base factor and $f_{B_0} = f_I$. Each detail factor is quantized with quantization depth $\frac{(\mathcal{M}-\mathcal{B})}{n}$, yielding the remaining tokens, as illustrated in Figure 2a. The full algorithm for extracting token maps from a given image is presented in Algorithm 1.

3.3. Iterative Detail Learning

We employ an auto-regressive approach to predict each successive “next-detail” token map. Given the set of tokens $\{r_1, r_2, \dots, r_{\mathcal{M}}\}$, the autoregressive likelihood is defined as,

$$P(r_1, \dots, r_{\mathcal{M}}) = \prod_{m=1}^{\mathcal{M}} P(r_m | r_1, \dots, r_{m-1}). \quad (13)$$

where each autoregressive unit, $r_m \in [V]^{h_m \times w_m}$ is a token map containing $h_m \times w_m$ tokens.

For the model architecture, we utilize a standard decoder-only Transformer architecture similar to that in GPT-2 [31], VQ-GAN [12], and VAR [39]. At each autoregressive step, the Transformer decoder predicts the distribution over all $h_m \times w_m$ tokens in parallel as depicted in Figure 2b. To enforce causality, as in [39], we apply a causal attention mask, ensuring that each token map r_m only attends to its preceding tokens $r_{\leq m}$.

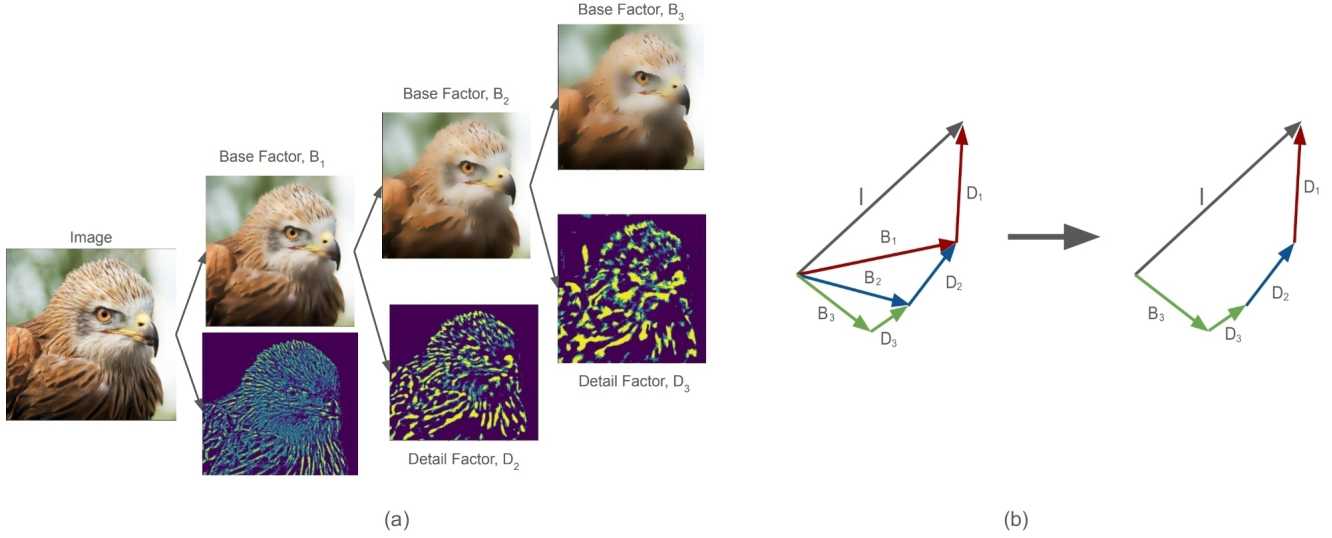


Figure 3. (a) Hierarchical Base-Detail Decomposition of an Image. (b) Representation of Image I in terms of base and detail factors.

Algorithm 1 Base-Detail VQ-VAE Encoding

Input:

- Raw image, I
- Base Image, B_n

Hyperparameters:

- Total number of tokens to represent the image, \mathcal{M}
- number of base tokens, \mathcal{B}
- number of detail factors, n

```

 $f_I \leftarrow \varepsilon(I)$ 
 $f_B \leftarrow \varepsilon(B)$ 
 $f_{D_i} \leftarrow f_{B_{i-1}} - f_{B_i} \forall i \in \{1, \dots, n\}$ 
 $t \leftarrow -1$ 
for  $k=1:\mathcal{M}$ :
  if  $k \leq \mathcal{B}$  then
     $r_k \leftarrow \mathcal{Q}(\text{interpolate}(f_B, h_k, w_k))$ 
     $R \leftarrow \text{queue}_{push}(R, r_k)$ 
     $z_k \leftarrow \text{LookUp}(r_k, \mathcal{Z})$ 
     $z_k \leftarrow \text{interpolate}(z_k, h_k, w_k)$ 
     $f_I \leftarrow f_I - \phi(z_k)$ 
     $f_B \leftarrow f_B - \phi(z_k)$ 
  else
    if  $\text{mod}(k, \frac{\mathcal{M}-\mathcal{B}}{n}) = 0$  then
       $t \leftarrow t + 1$ 
    end if
     $r_k \leftarrow \mathcal{Q}(f_{D_t})$ 
     $R \leftarrow \text{queue}_{push}(R, r_k)$ 
     $z_k \leftarrow \text{LookUp}(r_k, \mathcal{Z})$ 
     $f_I \leftarrow f_I - \phi(z_k)$ 
     $f_D \leftarrow f_D - \phi(z_k)$ 
  end if
end for
return base-detail tokens  $R$ .

```

Algorithm 2 Base-Detail VQ-VAE Reconstruction

Input: Base-Detail Tokens, R .

Hyperparameters:

- Total number of tokens to represent the image, \mathcal{M}
- number of base tokens, \mathcal{B}
- number of detail factors, n

```

 $\hat{f} \leftarrow 0$ 
for  $k=1:\mathcal{M}$  do:
  if  $k \leq \mathcal{B}$  then:
     $r_k \leftarrow \text{queue}_{pop}(R)$ 
     $z_k \leftarrow \text{lookup}(Z, r_k)$ 
     $z_k \leftarrow \text{interpolate}(z_k, h_k, w_k)$ 
     $\hat{f} \leftarrow \hat{f} + \phi_k(z_k)$ 
  else
     $r_k \leftarrow \text{queue}_{pop}(R)$ 
     $z_k \leftarrow \text{lookup}(Z, r_k)$ 
     $\hat{f} \leftarrow \hat{f} + \phi_k(z_k)$ 
  end if
end for
 $\hat{I} \leftarrow \mathcal{D}(\hat{f})$ 
return reconstructed image  $\hat{I}$ 

```

4. Experiments

4.1. Implementation Details

In order to get the detail decomposition of the training image, the Mumford-Shah smoothing operation as described in Equation 8 with $\alpha = 10$ and $\lambda = 0.01$ is utilized. Each training image is decomposed iteratively such that a 3rd order decomposition is obtained, $I = B_3 + D_3 + D_2 + D_1$. A Vanilla VQ-VAE [41] is used along with \mathcal{Z} extra con-

volution to realize the Base-Detail quantization scheme as depicted in Figure 2a and Algorithm 1. The base and detail factors all share the same code book with $V = 4096$. As in [12, 39], the tokenizer is trained on OpenImages [21] with Compound loss (Equation 6) and spatial downsample of $16\times$.

The tokenized base-detail factors as obtained by using Algorithm 1 are then utilized to train a Transformer Decoder architecture which learns to predict the “next-detail” token. A standard decoder-only transformer architecture is used similar to GPT-2 [31] and VQGAN [12]. During inference, the Transformer predicts the codes and the VQ-VAE decoder, $\mathcal{D}(\cdot)$ is utilized to obtain the generated image. The decoding algorithm is summarized in Algorithm 2. The depth of the transformer in CART is varied from 16 to 30 to obtain models with varying complexity and learning capability. The model is trained with a initial learning rate of 1^{-4} .

4.2. Empirical Results

The proposed CART model was evaluated on the ImageNet dataset [10] at resolutions of 256×256 (CART-256) and 512×512 (CART-512) to benchmark its performance against state-of-the-art (SOTA) methods in image generation. The comparative results are presented in Tables 1 and 2. We observe that the proposed CART model out-performs the SOTA VAR approach [39] and also achieves FID lower than that of the ImageNet validation set, all while maintaining comparable complexity and number of steps. Unlike VAR, the CART model benefits from the base-detail decomposition allowing it to dis-entangle the global structures from the local details. This makes the learning process easier, defining a more natural order of tokens. Figure 4 depicts some of the generated images using the proposed CART method and Figure 5 shows a comparison of images generated by VAR [39] and CART. It is evident from Figure 5 that CART leads to generated images with enhanced details and structure as compared to VAR which does not use a “next-detail” prediction scheme. Note that CART surpasses both Diffusion Transformer [1, 30] as well as the SOTA VAR model [39] in AutoRegressive Image generation.

4.2.1 Generalizing to Higher Resolutions

A significant advantage of using a base-detail decomposition is the disentanglement of global and local image features. This separation enables the model to generate high-resolution images, even when trained on lower-resolution

Type	Model	FID	IS	Params	Steps
GAN	BigGAN [4]	6.95	224.5	112M	1
GAN	GigaGAN [17]	3.45	225.5	569M	1
GAN	StyleGAN-XL [36]	2.30	265.1	166M	1
Diff.	ADM [11]	10.94	101.0	554M	250
Diff.	CDM [16]	4.88	158.7	-	8100
Diff.	LDM-4-G [34]	3.60	247.7	400M	250
Diff.	DiT-XL/2 [30]	2.27	278.2	675M	250
Diff.	L-DiT-3B [1]	2.10	304.4	3.0B	250
Diff.	L-DiT-7B [1]	2.28	316.2	7.0B	250
Mask	MaskGIT [7]	6.18	182.1	227M	8
Mask	RCG [24]	3.49	215.5	502M	20
AR	VQVAE-2 [33]	31.11	-	13.5B	5120
AR	VQGAN-re [12]	5.20	280.3	1.4B	256
AR	ViTVQ-re [44]	3.04	227.4	1.7B	1024
AR	RQTran-re [22]	3.80	323.7	3.8B	68
VAR	VAR-d16 [39]	3.30	274.4	310M	10
VAR	VAR-d30 [39]	1.92	323.1	2B	10
VAR	VAR-d30-re [39]	1.73	350.2	2B	10
VAR	VAR-d30-re [39]	1.70	350.2	2B	14
CART	CART-d16	3.02	284.0	310M	14
CART	CART-d24	1.98	318.6	1.0B	14
CART	CART-d24-re	1.82	338.9	1.0B	14
CART	CART-d30	1.67	366.8	2.0B	14
CART	CART-d30-re	1.60	372.4	2.0B	14
	(val. data)	1.78	236.9		

Table 1. Generative Models Comparison on ImageNet 256×256 . Suffix ‘-re’ refers to models that use rejection sampling

inputs. Empirically, we observe that the base factor encapsulates global features—such as class-conditional structure and overall color composition—while the detail factor captures local features, such as textures and fine-grained details. Consequently, the base factor can be upscaled without compromising essential global information, while the detail factor can be generated in a patchwise manner. Patchwise generation of details does not introduce discontinuities, as the patches in the detail factor inherently lack dependencies on global relationships across the image. Figure 6 depicts the comparison of bilinear resizing against images gener-



Figure 4. Generated Samples using CART-256



Figure 5. Comparison of samples generated by VAR-256 (top) and CART-256 (bottom)

Type	Model	FID	IS
GAN	BigGAN [4]	8.43	177.9
Diff.	ADM [11]	23.24	101.0
Diff.	DiT-XL/2 [30]	3.04	240.8
Mask	MaskGiT [7]	7.32	156.0
AR	VQGAN [12]	26.52	66.8
VAR	VAR-d36-s [39]	2.63	303.2
CART	CART-256-d30	2.93	295.6
CART	CART-512-d30	2.59	310.1

Table 2. Generative Models Comparison on ImageNet 512×512 .

ated using the method described above.

ImageNet 512×512 is utilized to evaluate the high-resolution capability of the CART Model with and without re-training the entire model from scratch. Table 2 summarizes the performance of our models as compared to SOTA on ImageNet- 512×512 . “CART-256” in Table 2 refers to high-resolution image generation as described above (without re-training), and “CART-512” refers to model trained from scratch using 512×512 training images.

4.3. Ablation Study

In Table 3 we evaluate the impact of the various components of the proposed CART model. Specifically, we observe that



Figure 6. Comparison of High Resolution (512×512) images as generated by left: bilinear resizing of CART-256 output and right: bilinear resizing of base factor and patchwise detail addition at 512×512

Model	CFG	MS Tokens	BD Tokens	FID
AR [12]	✗	✗	✗	18.65
VAR-d16 [39]	✓	✓	✗	3.30
CART-d16	✓	✗	✓	3.43
CART-d16	✓	✓	✓	3.02
VAR-d30 [39]	✓	✓	✗	1.73
CART-d30	✓	✓	✓	1.62

Table 3. Ablation Study of CART

the best performance is achieved when the Base factor is learned in a multi-scale fashion and the details are added at the final image resolution.

In Table 4 we compare the performance of proposed CART model when different order of decomposition is used for the learning process. Decomposition order of 0 is equivalent to using no detail decomposition and hence is the special case of VAR. We observe that the best performance is achieved when we utilize a 3^{rd} order Base-Detail decomposition. When the base detail decomposition is taken beyond the 3^{rd} order, the base image becomes over smooth and begins to lose essential details related to global struc-

Decomposition Order	FID
0 (Special case of VAR)	1.73
1	1.68
2	1.66
3	1.62
4	1.64

Table 4. Impact of decomposition order on performance of the CART model

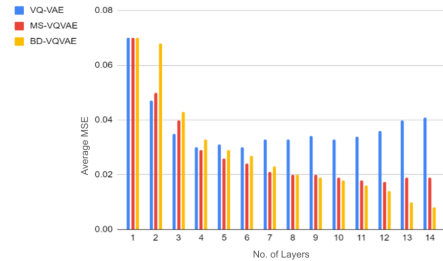


Figure 7. Comparison of Reconstruction MSE of Standard VQ-VAE (blue), Multiscale VQ-VAE (red) and Base-Detail VQ-VAE (yellow)

ture, leading to sub-optimal learning.

As evidenced in Figure 7, the reconstruction capability of the Base-Detail-VQ-VAE is significantly higher compared to the vanilla VQ-VAE [41] as well as the MS-VQVAE [39], specifically at higher depth of the VQ-VAE.

5. Conclusion

In this work, we proposed a novel approach to image synthesis through an auto-regressive (AR) framework that incorporates a “next-detail” prediction strategy, advancing the capabilities of AR models in high-resolution image generation. By leveraging a structured base-detail decomposition, our method enables iterative refinement that aligns with the natural hierarchical structure of images, effectively separating global from local features. Our contributions include a robust tokenization scheme which quantizes base and detail layers separately, preserving spatial integrity and enabling an effective AR process. Experimental results demonstrate that our approach not only achieves state-of-the-art performance in AR-based image generation but also reduces the computational complexity typically associated with scaling high-resolution outputs. Furthermore, we address limitations seen in conventional next-token and next-scale prediction methods, achieving a more accurate and efficient generative process.

In conclusion, our next-detail AR modeling framework introduces a scalable and computationally efficient approach to image synthesis, offering a compelling alternative to diffusion models and other state-of-the-art methods.

References

- [1] Alpha-vllm. large-dit-imagenet. <https://github.com/Alpha-VLLM/LLaMA2-Accessory/tree/f7fe19834b23e38f333403b91bb0330afe19f79e/Large-DiT-ImageNet>. Accessed: 2010-09-30. 6
- [2] Luigi Ambrosio and Vincenzo Maria Tortorelli. Approximation of functional depending on jumps by elliptic functional via t-convergence. *Communications on Pure and Applied Mathematics*, 43(8):999–1036, 1990. 3
- [3] Titas Anciukevičius, Zexiang Xu, Matthew Fisher, Paul Henderson, Hakan Bilen, Niloy J Mitra, and Paul Guerrero. Renderdiffusion: Image diffusion for 3d reconstruction, inpainting and generation. In *Proceedings of the IEEE/CVF conference on computer vision and pattern recognition*, pages 12608–12618, 2023. 2
- [4] Andrew Brock. Large scale gan training for high fidelity natural image synthesis. *arXiv preprint arXiv:1809.11096*, 2018. 6, 7
- [5] Tim Brooks, Aleksander Holynski, and Alexei A Efros. Instructpix2pix: Learning to follow image editing instructions. In *Proceedings of the IEEE/CVF Conference on Computer Vision and Pattern Recognition*, pages 18392–18402, 2023. 2
- [6] Tom B Brown. Language models are few-shot learners. *arXiv preprint arXiv:2005.14165*, 2020. 2
- [7] Huiwen Chang, Han Zhang, Lu Jiang, Ce Liu, and William T Freeman. Maskgit: Masked generative image transformer. In *Proceedings of the IEEE/CVF Conference on Computer Vision and Pattern Recognition*, pages 11315–11325, 2022. 6, 7
- [8] Mark Chen, Alec Radford, Rewon Child, Jeffrey Wu, Heewoo Jun, David Luan, and Ilya Sutskever. Generative pre-training from pixels. In *International conference on machine learning*, pages 1691–1703. PMLR, 2020. 2
- [9] Ciprian Corneanu, Raghudeep Gadde, and Aleix M Martinez. Latentpaint: Image inpainting in latent space with diffusion models. In *Proceedings of the IEEE/CVF Winter Conference on Applications of Computer Vision*, pages 4334–4343, 2024. 2
- [10] Jia Deng, Wei Dong, Richard Socher, Li-Jia Li, Kai Li, and Li Fei-Fei. Imagenet: A large-scale hierarchical image database. In *2009 IEEE conference on computer vision and pattern recognition*, pages 248–255. Ieee, 2009. 6
- [11] Prafulla Dhariwal and Alexander Nichol. Diffusion models beat gans on image synthesis. *Advances in neural information processing systems*, 34:8780–8794, 2021. 6, 7
- [12] Patrick Esser, Robin Rombach, and Bjorn Ommer. Taming transformers for high-resolution image synthesis. In *Proceedings of the IEEE/CVF conference on computer vision and pattern recognition*, pages 12873–12883, 2021. 2, 4, 6, 7, 8
- [13] Ian Goodfellow, Jean Pouget-Abadie, Mehdi Mirza, Bing Xu, David Warde-Farley, Sherjil Ozair, Aaron Courville, and Yoshua Bengio. Generative adversarial networks. *Communications of the ACM*, 63(11):139–144, 2020. 1, 2
- [14] Karol Gregor, Ivo Danihelka, Alex Graves, Danilo Rezende, and Daan Wierstra. Draw: A recurrent neural network for image generation. In *International conference on machine learning*, pages 1462–1471. PMLR, 2015. 2
- [15] Jonathan Ho, Ajay Jain, and Pieter Abbeel. Denoising diffusion probabilistic models. *Advances in neural information processing systems*, 33:6840–6851, 2020. 1, 2
- [16] Jonathan Ho, Chitwan Saharia, William Chan, David J Fleet, Mohammad Norouzi, and Tim Salimans. Cascaded diffusion models for high fidelity image generation. *Journal of Machine Learning Research*, 23(47):1–33, 2022. 2, 6
- [17] Minguk Kang, Jun-Yan Zhu, Richard Zhang, Jaesik Park, Eli Shechtman, Sylvain Paris, and Taesung Park. Scaling up gans for text-to-image synthesis. In *Proceedings of the IEEE/CVF Conference on Computer Vision and Pattern Recognition*, pages 10124–10134, 2023. 6
- [18] Tero Karras, Samuli Laine, and Timo Aila. A style-based generator architecture for generative adversarial networks. In *Proceedings of the IEEE/CVF conference on computer vision and pattern recognition*, pages 4401–4410, 2019. 3
- [19] Bahjat Kawar, Shiran Zada, Oran Lang, Omer Tov, Huiwen Chang, Tali Dekel, Inbar Mosseri, and Michal Irani. Imagic: Text-based real image editing with diffusion models. In *Proceedings of the IEEE/CVF Conference on Computer Vision and Pattern Recognition*, pages 6007–6017, 2023. 2
- [20] Diederik P Kingma. Auto-encoding variational bayes. *arXiv preprint arXiv:1312.6114*, 2013. 1, 2
- [21] Alina Kuznetsova, Hassan Rom, Neil Alldrin, Jasper Uijlings, Ivan Krasin, Jordi Pont-Tuset, Shahab Kamali, Stefan Popov, Matteo Mallocci, Alexander Kolesnikov, et al. The open images dataset v4: Unified image classification, object detection, and visual relationship detection at scale. *International journal of computer vision*, 128(7):1956–1981, 2020. 6
- [22] Doyup Lee, Chiheon Kim, Saehoon Kim, Minsu Cho, and Wook-Shin Han. Autoregressive image generation using residual quantization. In *Proceedings of the IEEE/CVF Conference on Computer Vision and Pattern Recognition*, pages 11523–11532, 2022. 4, 6
- [23] Haoying Li, Yifan Yang, Meng Chang, Shiqi Chen, Huajun Feng, Zhihai Xu, Qi Li, and Yueting Chen. Srdiff: Single image super-resolution with diffusion probabilistic models. *Neurocomputing*, 479:47–59, 2022. 2
- [24] Tianhong Li, Dina Katabi, and Kaiming He. Self-conditioned image generation via generating representations. *arXiv preprint arXiv:2312.03701*, 2023. 6
- [25] Andreas Lugmayr, Martin Danelljan, Andres Romero, Fisher Yu, Radu Timofte, and Luc Van Gool. Repaint: Inpainting using denoising diffusion probabilistic models. In *Proceedings of the IEEE/CVF conference on computer vision and pattern recognition*, pages 11461–11471, 2022. 2
- [26] Larry R Medsker, Lakhmi Jain, et al. Recurrent neural networks. *Design and Applications*, 5(64-67):2, 2001. 2
- [27] Mehdi Mirza. Conditional generative adversarial nets. *arXiv preprint arXiv:1411.1784*, 2014. 1, 2
- [28] David Bryant Mumford and Jayant Shah. Optimal approximations by piecewise smooth functions and associated variational problems. *Communications on pure and applied mathematics*, 1989. 3

- [29] Niki Parmar, Ashish Vaswani, Jakob Uszkoreit, Lukasz Kaiser, Noam Shazeer, Alexander Ku, and Dustin Tran. Image transformer. In *International conference on machine learning*, pages 4055–4064. PMLR, 2018. 2
- [30] William Peebles and Saining Xie. Scalable diffusion models with transformers. In *Proceedings of the IEEE/CVF International Conference on Computer Vision*, pages 4195–4205, 2023. 6, 7
- [31] Alec Radford, Jeffrey Wu, Rewon Child, David Luan, Dario Amodei, Ilya Sutskever, et al. Language models are unsupervised multitask learners. *OpenAI blog*, 1(8):9, 2019. 2, 4, 6
- [32] Aditya Ramesh, Mikhail Pavlov, Gabriel Goh, Scott Gray, Chelsea Voss, Alec Radford, Mark Chen, and Ilya Sutskever. Zero-shot text-to-image generation. In *International conference on machine learning*, pages 8821–8831. Pmlr, 2021. 2
- [33] Ali Razavi, Aaron Van den Oord, and Oriol Vinyals. Generating diverse high-fidelity images with vq-vae-2. *Advances in neural information processing systems*, 32, 2019. 6
- [34] Robin Rombach, Andreas Blattmann, Dominik Lorenz, Patrick Esser, and Björn Ommer. High-resolution image synthesis with latent diffusion models. In *Proceedings of the IEEE/CVF conference on computer vision and pattern recognition*, pages 10684–10695, 2022. 6
- [35] Tim Salimans, Andrej Karpathy, Xi Chen, and Diederik P Kingma. Pixelcnn++: Improving the pixelcnn with discretized logistic mixture likelihood and other modifications. *arXiv preprint arXiv:1701.05517*, 2017. 2
- [36] Axel Sauer, Katja Schwarz, and Andreas Geiger. Stylegan-xl: Scaling stylegan to large diverse datasets. In *ACM SIGGRAPH 2022 conference proceedings*, pages 1–10, 2022. 6
- [37] Huajie Shao, Shuochao Yao, Dachun Sun, Aston Zhang, Shengzhong Liu, Dongxin Liu, Jun Wang, and Tarek Abdelzaher. Controlvae: Controllable variational autoencoder. In *International conference on machine learning*, pages 8655–8664. PMLR, 2020. 1, 2
- [38] Jiaming Song, Chenlin Meng, and Stefano Ermon. Denoising diffusion implicit models. *arXiv preprint arXiv:2010.02502*, 2020. 1, 2
- [39] Keyu Tian, Yi Jiang, Zehuan Yuan, Bingyue Peng, and Liwei Wang. Visual autoregressive modeling: Scalable image generation via next-scale prediction. *arXiv preprint arXiv:2404.02905*, 2024. 2, 4, 6, 7, 8
- [40] Aäron Van Den Oord, Nal Kalchbrenner, and Koray Kavukcuoglu. Pixel recurrent neural networks. In *International conference on machine learning*, pages 1747–1756. PMLR, 2016. 2
- [41] Aaron Van Den Oord, Oriol Vinyals, et al. Neural discrete representation learning. *Advances in neural information processing systems*, 30, 2017. 2, 3, 5, 8
- [42] A Vaswani. Attention is all you need. *Advances in Neural Information Processing Systems*, 2017. 2
- [43] Shiyuan Yang, Xiaodong Chen, and Jing Liao. Uni-paint: A unified framework for multimodal image inpainting with pretrained diffusion model. In *Proceedings of the 31st ACM International Conference on Multimedia*, pages 3190–3199, 2023. 2
- [44] Jiahui Yu, Xin Li, Jing Yu Koh, Han Zhang, Ruoming Pang, James Qin, Alexander Ku, Yuanzhong Xu, Jason Baldridge, and Yonghui Wu. Vector-quantized image modeling with improved vqgan. *arXiv preprint arXiv:2110.04627*, 2021. 6
- [45] Zongsheng Yue, Jianyi Wang, and Chen Change Loy. Resshift: Efficient diffusion model for image super-resolution by residual shifting. *Advances in Neural Information Processing Systems*, 36, 2024. 2
- [46] Chenshuang Zhang, Chaoning Zhang, Mengchun Zhang, and In So Kweon. Text-to-image diffusion models in generative ai: A survey. *arXiv preprint arXiv:2303.07909*, 2023. 2
- [47] Richard Zhang, Phillip Isola, Alexei A Efros, Eli Shechtman, and Oliver Wang. The unreasonable effectiveness of deep features as a perceptual metric. In *Proceedings of the IEEE conference on computer vision and pattern recognition*, pages 586–595, 2018. 3
- [48] Zhizhuo Zhou and Shubham Tulsiani. Sparsefusion: Distilling view-conditioned diffusion for 3d reconstruction. In *Proceedings of the IEEE/CVF Conference on Computer Vision and Pattern Recognition*, pages 12588–12597, 2023. 2
- [49] Yuanzhi Zhu, Zhaohai Li, Tianwei Wang, Mengchao He, and Cong Yao. Conditional text image generation with diffusion models. In *Proceedings of the IEEE/CVF Conference on Computer Vision and Pattern Recognition*, pages 14235–14245, 2023. 2